

# Multipolar Fermi Surface Deformations in $\text{Sr}_2\text{RuO}_4$ Probed by Resistivity and Sound Attenuation: A Window into Electron Viscosity and the Collision Operator

Davis Thuillier,<sup>1</sup> Sayak Ghosh,<sup>2,3</sup> B. J. Ramshaw,<sup>4,5,6,\*</sup> and Thomas Scaffidi<sup>1,6,†</sup>

<sup>1</sup>*Department of Physics, University of California, Irvine, Irvine, CA 92697, USA*

<sup>2</sup>*Geballe Laboratory for Advanced Materials, Stanford University, Stanford, CA, USA*

<sup>3</sup>*Department of Applied Physics, Stanford University, Stanford, CA, USA*

<sup>4</sup>*Laboratory of Atomic and Solid State Physics, Cornell University, Ithaca, NY, USA*

<sup>5</sup>*Canadian Institute for Advanced Research, Toronto, Ontario, Canada*

<sup>6</sup>*These authors contributed equally to this work.*

(Dated: March 10, 2025)

Recent developments in electron hydrodynamics have demonstrated the importance of considering the full structure of the electron-electron scattering operator, which encodes a sequence of lifetimes, one for each component of the Fermi surface deformation in a multipolar expansion. In this context, the dipolar lifetime is measured by resistivity, whereas the quadrupolar component probes the viscosity and can be measured in the bulk via sound attenuation. We introduce a framework to extract the collision operator of an arbitrary metal by combining resistivity and sound attenuation measurements with a realistic calculation of the scattering operator that includes multiband and Umklapp effects. The collision operator allows for the prediction of a plethora of properties, including the non-local conductivity, and can be used to predict hydrodynamic behavior for bulk metals. As a first application, we apply this framework to  $\text{Sr}_2\text{RuO}_4$  in a temperature range where electron-electron scattering is dominant. We find quantitative agreement between our model and the temperature dependence of both the resistivity and the sound attenuation, we extract the ratio of the quadrupolar ( $B_{1g}$ ) to dipolar relaxation rate to be 1.3, and we predict a strongly anisotropic non-local conductivity arising from the  $\alpha$  and  $\beta$  bands.

Particle flow is hydrodynamic when the collisions between particles conserve energy, momentum, and particle number [1]. This is the case for liquid water, but for electrons in a metal, collisions with the lattice relax momentum and the flow is typically diffusive (i.e. Ohmic). Gurzhi [2] showed that hydrodynamic effects should contribute to the electrical resistivity when momentum-conserving (i.e. non-Umklapp) electron-electron collisions dominate over other types of scattering. Under this condition, the electron viscosity—which controls the diffusion of momentum in the electron fluid—can become a relevant quantity in electric transport measurements [2–14].

Electron viscosity, however, has no impact on *bulk* electric transport. Instead, it only enters in *size-restricted* transport, for which the boundary of the device ultimately acts as the dominant momentum “sink” in the system [15–34]. The reason why the viscosity does not contribute to bulk electric transport is fundamental: conductivity and viscosity probe the relaxation of different deformation modes of the Fermi surface (see Figure 1). Specifically, the bulk conductivity probes the relaxation of a dipolar Fermi surface (FS) deformation that is proportional to the Fermi velocity, e.g.  $v_x \propto \cos(\theta)$  for a circular FS, with  $\theta$  the angle around the FS. By contrast, the electron viscosity is sensitive to the relaxation of quadrupolar FS deformations, e.g. varying as  $\cos(2\theta)$ .

Quadrupolar FS deformations are orthogonal to dipolar electrical currents in the bulk due their distinct symmetries. Viscosity can, however, contribute to electric resistance in size-restricted samples because translation

symmetry breaking at the sample boundary generates quadrupolar (and higher-order multipolar) FS deformations [2, 17]. These deformations clearly depend on details of how electrons interact with sample boundaries, and thus a more direct way to probe electron viscosity would be to generate *bulk* quadrupolar FS deformations: these are the deformations generated by sound waves.

Schematically, sound waves traveling through a metal distort the lattice and change the electronic band structure through the deformation potentials [37, 38], leading to quadrupolar deformations of the Fermi surface, with no net current (e.g.  $D_{B_{1g}} \propto \cos(2\theta)$ , see Figure 1). At low temperatures, where phonon-phonon and phonon-dislocation scattering are weak (typically below about 20 kelvin), and in the limit of long sound wavelength (compared to the electronic mean free path), the sound attenuation coefficient  $\alpha$ —typically expressed in nepers, or  $\approx 8.7$  dB, per meter—is dominated by the equilibration of the conduction electrons to the deformed lattice potential [38, 39]. In keeping with the conventions of the ultrasonic literature, this long-wavelength regime is referred to as the “hydrodynamic” regime [38], and the attenuation coefficient is typically expressed as an “acoustic viscosity”:  $\eta = \alpha \rho v_s / q^2$ , where  $\rho$  is the material density,  $v_s$  is the sound velocity, and  $q$  is the sound wavevector. These definitions should not be confused with the contemporary uses of the words “hydrodynamic” and “viscosity” in the context of transport experiments, where these terms refer solely to the electronic sub-system [14]. For clarity, we will henceforth distinguish between “transport” and “acoustic” viscosities. In the simplest cases of a circu-

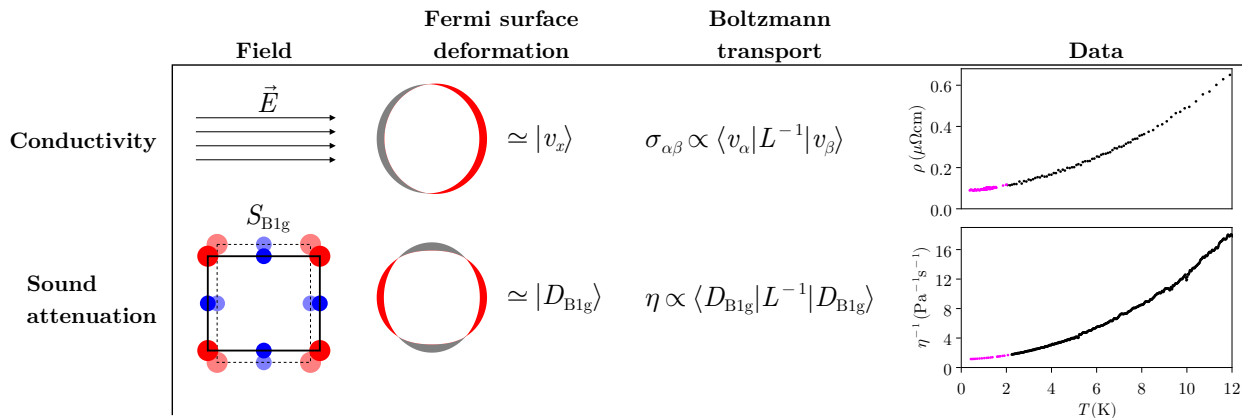


FIG. 1. **Schematic comparison of electrical conductivity with sound attenuation.** The Fermi surface deforms under an applied field, here an electric field for conductivity and a strain field for sound attenuation (red and gray regions correspond to population and depopulation, respectively). The Fermi surface deformation relevant to the conductivity,  $\sigma$ , is proportional to the Fermi velocity  $v_\alpha(\mathbf{k})$  and is thus dipolar in nature; in contrast, the Fermi surface deformation relevant for sound attenuation,  $\eta$ , is determined by the deformation potential,  $D_{\alpha\beta}(\mathbf{k})$ , and is quadrupolar. Both conductivity and sound attenuation are calculated by evaluating the expectation value of the inverse collision operator,  $L^{-1}$ . The final column shows measurements of the resistivity (reproduced from Lupien [35]) and the inverse sound attenuation of  $\text{Sr}_2\text{RuO}_4$ : both quantities show Fermi liquid  $T^2$  scaling. Data shown in pink are reproduced from Lupien *et al.* [36] and taken in a 1.5 T magnetic field to suppress the superconducting transition.

lar FS, the acoustic viscosity is equal to the transport viscosity up to a constant of proportionality related to the average deformation potential (See End Matter for a discussion of the more general case).

Consequently, the acoustic viscosity is proportional to the relaxation time for quadrupolar modes ( $\eta \propto \tau_2$ ), whereas the conductivity is proportional to the transport mean free time ( $\sigma \propto \tau_1$ ) that measures the relaxation of dipolar modes (See Figure 1). Prior studies in elemental metals [40–45] have focused on the ratio  $\tau_2/\tau_1$ , but only in a regime for which either electron-impurity or electron-phonon scattering dominate [46]. Here, we are interested in the temperature regime that is dominated by electron-electron scattering, for which a parametric difference between the two rates is possible because the relaxation of currents requires Umklapp scattering [47], whereas the acoustic attenuation does not.

More generally, conductivity and viscosity probe the first two modes in a “Fermi surface harmonics” expansion (generalizing cylindrical or spherical harmonics to the case of an arbitrary FS shape) that encodes a hierarchy of timescales  $\tau_l$  (with  $l$  a generalized mode index) over which multipolar FS deformations relax. Based on this fact, we propose to combine measurements of electrical conductivity and acoustic viscosity with theoretical calculations in order to construct the entire *collision operator*, which is the central object in studies of novel regimes of transport [17, 48–54].

The fine features of the collision operator were neglected for a long time due to the widespread use of the single relaxation time approximation (RTA), for which  $\tau_l = \tau$  for all  $l$ . This approximation was subsequently

improved through the use of a two-rate model, for which the hydrodynamic regime is reached when  $\tau_2^{-1}/\tau_1^{-1} \gg 1$  [17, 48, 55], and more recently through the discovery of a tomographic regime for 2D metals [49, 50, 52–54]. However, even these more recent works have typically used simplistic models when calculating the collision operator (e.g. isotropic Fermi surfaces, no Umklapp) [8–10, 17, 22, 23, 49, 52, 54–56]. While this might be justified in low-density conductors like two-dimensional electron gases [17, 57, 58] or graphene [4, 11, 12], it is not applicable to many other candidate materials. A calculation of the scattering operator for realistic band structures is thus needed if we intend to find new materials with hydrodynamic regimes, and more generally if we are to understand the fundamental properties of scattering in metals, strange or not [59–61].

As a proof of principle, we apply this framework to  $\text{Sr}_2\text{RuO}_4$ —a well-characterized Fermi liquid with moderately strong electron-electron interactions [62–74]. We are interested in a temperature regime below  $\sim 12$  K [75] for which both resistivity (taken from from Lupien [35]) and inverse  $B_{1g}$  viscosity (as measured here using resonant ultrasound spectroscopy, see below) follow conventional Fermi liquid scaling (i.e. grow quadratically with temperature, see Figure 1 [76]).

We find the following fits to the experimental data shown in Figure 2:

$$\rho/\rho_0 = 1 + B_\rho T^2 \text{ and } \eta^{-1}/\eta_0^{-1} = 1 + B_{\eta^{-1}} T^2 \quad (1)$$

with  $B_\rho = 0.035/K^2$  and  $B_{\eta^{-1}} = 0.089/K^2$ .

The fact that  $B_\rho$  and  $B_{\eta^{-1}}$  differ by a factor of  $\sim 2.5$  is a clear indication of the failure of the single RTA, and

provides a very stringent consistency check on any theoretical model for electron scattering in this material. The remainder of this Letter will demonstrate how a state-of-the-art numerical calculation of the collision operator for a realistic band structure illuminates the physics behind the difference of these prefactors. We will then use the extracted collision operator to predict non-local transport properties.

Before proceeding with the analysis, we first provide details of the acoustic attenuation measurements (see also End Matter). To access the long-wavelength limit of sound attenuation in  $\text{Sr}_2\text{RuO}_4$ , we used resonant ultrasound spectroscopy (RUS). Following Ghosh *et al.* [77, 78], we measured all six elastic moduli and their respective attenuation coefficients, from 1.2 K to 12 K, of a single-crystal  $\text{Sr}_2\text{RuO}_4$  sample with a  $T_c$  of 1.43 K. Here, we focus on the  $B_{1g}$  viscosity because it is particularly large in  $\text{Sr}_2\text{RuO}_4$  due to the proximity of the  $\gamma$  Fermi surface to the van Hove points at the edge of the Brillouin zone. This produces an enhanced density of states along the (100) and (010) directions, for which the  $B_{1g}$  deformation potential is maximal [79]. By comparison, the  $B_{2g}$  viscosity does not even exceed the background in our experiment [78].

We take resistivity data from Lupien that was measured on a sample with a  $T_c$  between 1.41 K and 1.44 K. A sample cut from the same resistivity sample was used to perform pulse-echo sound attenuation measurements in Lupien *et al.* [36][80]. We find that  $\eta_{B_{1g}}$  measured by Lupien *et al.* [36] matches quantitatively with the  $\eta_{B_{1g}}$  we measure using RUS. This ensures that the elastic scattering rate in our sample and the sample of Lupien *et al.* [36] is very similar—a fact also evidenced by the very similar  $T_c$ 's of our samples. We use the measurements from Lupien *et al.* [36] made in a magnetic field to extend the viscosity below  $T_c$ .

*Collision operator*— In order to calculate the conductivity and viscosity, we first construct the collision operator entering the Boltzmann equation:

$$\partial_t f + \mathbf{v} \cdot \nabla_r f + \mathbf{F} \cdot \nabla_k f = -L[f], \quad (2)$$

with  $f$  the electron distribution function,  $L = L_{ee} + L_{\text{imp}}$  the collision operator including both electron-electron (e-e) and electron-impurity (e-imp) scattering,  $\mathbf{v}$  the Fermi velocity,  $\mathbf{k}$  momentum, and  $\mathbf{F}$  external forces. We consider weak perturbations of the Fermi-Dirac distribution away from equilibrium of the form  $f(\epsilon_{\mathbf{k}}) = f^{(0)}(\epsilon_{\mathbf{k}}) + \frac{-\partial f^{(0)}}{\partial \epsilon_{\mathbf{k}}} \chi(\mathbf{k})$ , where  $f^{(0)}$  denotes the equilibrium Fermi-Dirac distribution, and  $\chi(\mathbf{k})$  describes the perturbation away from equilibrium.

The electron-electron collision operator reads  $L_{ee}[\chi] \equiv$

$\int d\mathbf{k}' \mathcal{L}_{ee}(\mathbf{k}_1, \mathbf{k}') \chi(\mathbf{k}')$ , with the kernel given by

$$\begin{aligned} \mathcal{L}_{ee}(\mathbf{k}_1, \mathbf{k}') &= \left( \frac{\partial f^{(0)}}{\partial \epsilon_{\mathbf{k}_1}} \right)^{-1} \int_{\text{BZ}} \frac{d^2 \mathbf{k}_2 d^2 \mathbf{k}_3 d^2 \mathbf{k}_4}{(2\pi)^6} \\ &\times \Gamma(\mathbf{k}_1, \mathbf{k}_2, \mathbf{k}_3, \mathbf{k}_4) f^{(0)}(\mathbf{k}_1) f^{(0)}(\mathbf{k}_2) \overline{f^{(0)}(\mathbf{k}_3) f^{(0)}(\mathbf{k}_4)} \\ &\times (\delta(\mathbf{k}_1 - \mathbf{k}') + \delta(\mathbf{k}_2 - \mathbf{k}') - \delta(\mathbf{k}_3 - \mathbf{k}') - \delta(\mathbf{k}_4 - \mathbf{k}')) \end{aligned} \quad (3)$$

where  $\Gamma$  denotes the rate for the scattering process  $\mathbf{k}_1, \mathbf{k}_2 \rightarrow \mathbf{k}_3, \mathbf{k}_4$  and where  $\overline{f^{(0)}} \equiv 1 - f^{(0)}$ . We use a three-orbital, 2D Hubbard model for  $\text{Sr}_2\text{RuO}_4$ , in which case  $\Gamma$  is given by a multi-orbital generalization of the formula  $\Gamma = \frac{2\pi}{\hbar} U_{ee}^2 \delta(\mathbf{k}_1 + \mathbf{k}_2 - \mathbf{k}_3 - \mathbf{k}_4) \delta(\epsilon_{\mathbf{k}_1} + \epsilon_{\mathbf{k}_2} - \epsilon_{\mathbf{k}_3} - \epsilon_{\mathbf{k}_4})$  (see Supplemental Material (SM) [81] to this Letter for details). Extending the method of Refs. [65, 84], we numerically calculate the collision kernel of Eq. 3 for a discretized annular region of  $k$ -space centered on each Fermi surface and of width proportional to  $k_B T$ , with 4884 patches in total (see SM for more details). Generating the full collision operator at this resolution requires summing over  $\sim 10^{11}$  scattering processes.

We also include the electron-impurity scattering operator  $L_{\text{imp}}[\chi] \equiv \int d\mathbf{k}_2 \mathcal{L}_{\text{imp}}(\mathbf{k}_1, \mathbf{k}_2) \chi(\mathbf{k}_2)$  with

$$\mathcal{L}_{\text{imp}}(\mathbf{k}_1, \mathbf{k}_2) = \frac{2\pi}{\hbar} n_{\text{imp}} |\langle \mathbf{k}_1 | V_{\text{imp}} | \mathbf{k}_2 \rangle|^2 \delta(\epsilon_{\mathbf{k}_1} - \epsilon_{\mathbf{k}_2}) \quad (4)$$

where  $n_{\text{imp}}$  is the impurity density and  $V_{\text{imp}}$  measures the impurity potential strength. We assume scattering on point-like impurities in the unitary limit [85], following previous work on  $\text{Sr}_2\text{RuO}_4$  [86, 87]. In this limit, and for an isotropic 2D band,  $|\langle \mathbf{k}_1 | V_{\text{imp}} | \mathbf{k}_2 \rangle|^2 = 4\hbar^2 v_F^2 / k_F^2$  [88, 89]. We use a straightforward, multiband generalization of this formula, given in the SM.

To calculate the full collision operator, we combine the electron-electron and electron-impurity scattering contributions and treat the energy scales for each contribution ( $U_{ee}$  and  $U_{\text{imp}}$ ) as our only two fit parameters:

$$L = U_{ee}^2 \tilde{L}_{ee} + U_{\text{imp}}^2 \tilde{L}_{\text{imp}}, \quad (5)$$

with  $\tilde{L}_{ee} \equiv L_{ee}/U_{ee}^2$  and  $\tilde{L}_{\text{imp}} \equiv L_{\text{imp}}/U_{\text{imp}}^2$ , and where  $U_{\text{imp}}^2 \equiv n_{\text{imp}} a^{-2} |\langle V_{\text{imp}} \rangle|_{\text{av}}^2$  with  $a$  being the lattice spacing and  $|\langle V_{\text{imp}} \rangle|_{\text{av}}$  a band-averaged matrix element for electron-impurity scattering (see SM [81] for details).

With the collision operator in hand, the conductivity and acoustic viscosity are calculated as expectation values [38, 47]:

$$\begin{aligned} \sigma_{\alpha\beta} &= 2e^2 \langle v_\alpha | L^{-1} | v_\beta \rangle, \\ \eta_{\alpha\beta\gamma\delta} &= 2 \langle D_{\alpha\beta} | L^{-1} | D_{\gamma\delta} \rangle \end{aligned} \quad (6)$$

where  $v_\alpha = \hbar^{-1} \nabla_{k_\alpha} \epsilon_{\mathbf{k}}$  is the Fermi velocity,  $D_{\alpha\beta} = \frac{\partial \epsilon_{\mathbf{k}}}{\partial S_{\alpha\beta}}$  is the deformation potential [38][90], and  $\langle \psi | \chi \rangle \equiv \int_{\text{BZ}} \frac{d^2 \mathbf{k}}{(2\pi)^2} \frac{-\partial f^{(0)}}{\partial \epsilon_{\mathbf{k}}} \psi^*(\mathbf{k}) \chi(\mathbf{k})$ . The factors of 2 are due to spin. As mentioned above, we will focus on the  $B_{1g}$  viscosity, in which case  $|D_{B_{1g}}\rangle = \frac{1}{2} |D_{xx}\rangle - \frac{1}{2} |D_{yy}\rangle$ .

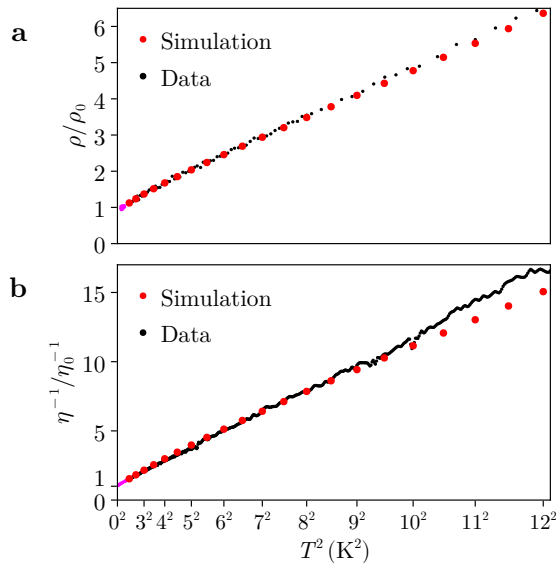


FIG. 2. **Comparison of experiment and theory for the resistivity (a) and inverse viscosity (b) as a function of temperature.** Two free parameters were adjusted to match  $\rho(T)$ ; those same two parameters are then used to calculate the normalized viscosity  $\eta^{-1}/\eta_0^{-1}$ , which shows excellent agreement with experiment. Resistivity data from [35], and viscosity data below 2 K from [36].

We first fit our two parameters to match the measured resistivity  $\rho(T)$  (Figure 2a) and obtain a good fit for  $U_{ee} = 0.074$  eV and  $U_{imp} = 4.8 \times 10^{-4}$  eV. Using the exact same parameters, we then predict the B1g viscosity and also find good agreement with experiments (Figure 2b). That the calculation predicts good agreement with experimental viscosity—using the parameters inferred from the resistivity—is nontrivial, since the experimental data clearly deviates from the single RTA as discussed above: over the temperature range we consider, the resistivity increases by a factor of 6 whereas the viscosity increases by a factor of 16. If the single RTA was valid, then both quantities would have the same relative increase.

*Effective relaxation times*—To highlight the breakdown of the single RTA, it is useful to define effective relaxation times corresponding to each quantity, analogous to  $\tau_1$  and  $\tau_2$  defined in the introduction. However, for an anisotropic, multi-band system like  $\text{Sr}_2\text{RuO}_4$ ,  $|v_\alpha\rangle$  and  $|D_{\alpha\beta}\rangle$  are, in general, not eigenmodes of  $L$ , thus conductivity and viscosity cannot be associated with a single eigenvalue of  $L$ . Nevertheless, effective lifetimes corresponding to the conductivity and the (B1g) viscosity can be defined based on (6) such that “generalized

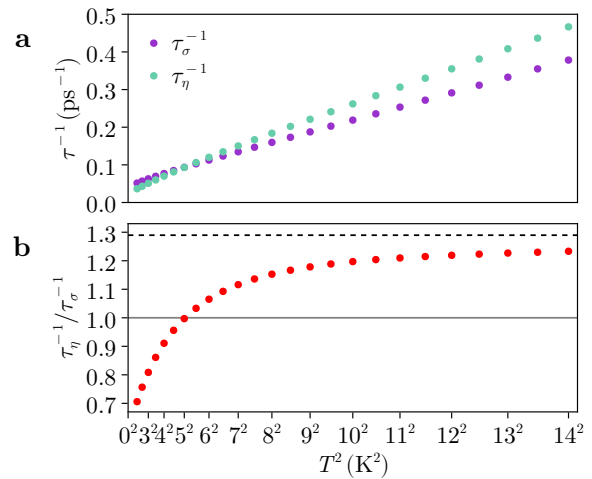


FIG. 3. **Effective inverse lifetimes extracted from the conductivity and viscosity (a), along with their ratio (b).** Panel a shows that both lifetimes grow roughly quadratically with  $T$ . Panel b shows that the ratio between lifetimes tends towards a value of approximately 1.3 at high temperature (dashed line). A ratio of 1 (solid line) is what is assumed within a single relaxation time approximation.

Drude formulas” hold:

$$\begin{aligned} \sigma &= 2e^2 \langle v_x | v_x \rangle \tau_\sigma \text{ with } \tau_\sigma \equiv \frac{\langle v_x | L^{-1} | v_x \rangle}{\langle v_x | v_x \rangle}, \\ \eta &= 2 \langle D_{\text{B1g}} | D_{\text{B1g}} \rangle \tau_\eta \text{ with } \tau_\eta \equiv \frac{\langle D_{\text{B1g}} | L^{-1} | D_{\text{B1g}} \rangle}{\langle D_{\text{B1g}} | D_{\text{B1g}} \rangle}. \end{aligned} \quad (7)$$

The breakdown of the single RTA is confirmed by comparing the effective lifetimes for each quantity, as shown in Figure 3. In panel a, we see that both inverse lifetimes grow like  $T^2$  but with a prefactor that is  $\sim 1.3$  times larger for  $\eta$  than for  $\sigma$ . Whereas e-e scattering can only contribute to the resistivity through Umklapp, there is no such constraint for the viscosity, so the ratio  $\frac{1}{1.3}$  is a proxy for the relative contribution of Umklapp processes compared to the total. There is thus no large separation between Umklapp and non-Umklapp rates in  $\text{Sr}_2\text{RuO}_4$ , which we attribute to the proximity of the  $\gamma$  band to the zone boundary. Note that was not obvious *a priori*, since the  $\alpha$  and  $\beta$  bands have substantially smaller Fermi wavevectors than  $\gamma$ , and interband Umklapp processes are thus key to understand transport in this material [91].

Moreover, identifying the condition  $\tau_\eta^{-1}/\tau_\sigma^{-1} \gg 1$  as analogous to  $\tau_2^{-1}/\tau_1^{-1} \gg 1$ , which is the figure of merit for hydrodynamics in the isotropic case [17, 48], we find that  $\tau_\eta^{-1}/\tau_\sigma^{-1}$  is at most 1.3. This precludes a deep hydrodynamic regime in  $\text{Sr}_2\text{RuO}_4$ .

Further, at low- $T$ , we note that the ratio of scattering rates is inverted: the effective scattering rate for the viscosity is smaller than that for the conductivity. This is due to a multi-band effect: at low- $T$ , electron-impurity

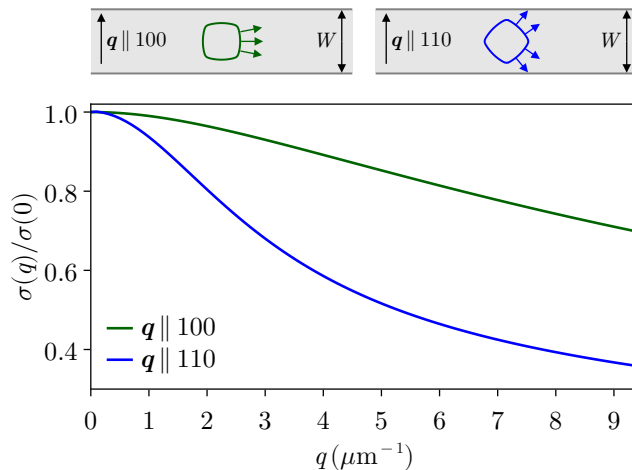


FIG. 4. **Non-local conductivity** calculated at  $T = 14$  K using the model parameters fit to the  $\text{Sr}_2\text{RuO}_4$  resistivity data. We predict a strong anisotropy depending on the orientation of  $\mathbf{q}$  (taken to be along the (100) or (110) crystallographic direction of  $\text{Sr}_2\text{RuO}_4$ ). Top: schematic showing the  $\beta$  FS and selected Fermi velocities within an effective “channel”, for the two  $\mathbf{q}$  directions we consider (the  $\alpha$  FS is oriented in the same way as  $\beta$ ).

scattering dominates. In the unitary limit, this leads to a smaller scattering rate on the  $\gamma$  band due to its higher effective mass. Since the weight on the  $\gamma$  band is comparatively higher for the deformation potential  $|D_{B_{1g}}|$  than for the current  $|v_x|$ , this leads to a comparatively smaller  $\tau_\eta^{-1}$  in the impurity-dominated regime at low temperature.

*Non-local conductivity*— There is considerable interest in predicting size-restricted conductivity because this experimental configuration has been used extensively as a probe electron viscosity. Now that we have an accurate collision operator, we could use it in a spatially-dependent Boltzmann calculation with appropriate boundary conditions for a given sample geometry. Such a calculation, however, would take us beyond the scope of this Letter. Instead, we can calculate the closely related non-local conductivity  $\sigma(\mathbf{q})$  [33, 92]:

$$\sigma_{\alpha\beta}(\mathbf{q}) = 2e^2 \langle v_\alpha | (L + i\mathbf{q} \cdot \mathbf{v})^{-1} | v_\beta \rangle. \quad (8)$$

Because it probes the flow of electrons in response to an electric field with transverse spatial modulation  $E_x = Ee^{iqy}$ , the transverse non-local conductivity  $\sigma(\mathbf{q})$  can be regarded as a proxy for the conductivity of electrons moving along  $x$  in a channel whose width along  $y$  is approximately half the electric field wavelength, i.e.  $W \sim \pi/q$  (see Figure 4 top panel). An additional class of experiments sensitive to  $\sigma(q)$  is electromagnetic measurements that involve a spatially-varying electric field in bulk samples [93, 94], e.g. using the skin effect [95–98].

Our prediction for  $\sigma(q)$  at  $T = 14$  K for  $q$  along (100) and (110), is shown in Figure 4. For each  $\mathbf{q}$  direc-

tion, fitting the small- $q$  decay of the non-local conductivity to  $\sigma(q) = \sigma(0)(1 - q^2/q_0^2 + \dots)$  uniquely defines an effective mean free path for non-local transport,  $q_0^{-1}$ . In the hydrodynamic limit, this definition recovers the usual Gurzhi length  $q_0^{-1} = \ell_{\text{Gurzhi}} = \sqrt{\nu^{\text{tr}}\tau_\sigma}$ , with  $\nu^{\text{tr}}$  the “transport viscosity” that would appear in an effective Stokes-Ohm description [2, 4]. As explained in the End Matter, the transport viscosity  $\nu^{\text{tr}}$  is subtly different from the “acoustic viscosity” considered above, although they both involve relaxation of modes in the same sector, namely  $B_{2g}$  for  $\mathbf{q}$  along (100) and  $B_{1g}$  for  $\mathbf{q}$  along (110). Interestingly, we find a factor of 2.5 anisotropy for the effective mean free paths, even at  $T = 14$  K for which electron-electron scattering dominates:  $q_{0,(100)}^{-1} = 0.1 \mu\text{m}$  and  $q_{0,(110)}^{-1} = 0.25 \mu\text{m}$  (corresponding to viscosities of  $\nu_{B_{2g}} = 0.0038 \text{ m}^2/\text{s}$  and  $\nu_{B_{1g}} = 0.024 \text{ m}^2/\text{s}$ , respectively). In analogy with earlier work on systems with polygonal Fermi surfaces like  $\text{PdCoO}_2$  [92, 99–103], we attribute this anisotropy to the square-like Fermi surfaces of the  $\alpha$  and  $\beta$  bands, which lead to an “easy direction” for  $\mathbf{q}$  along (100) for which the flat edges of the Fermi surface lead to a Fermi velocity dominantly oriented along the direction of current propagation (see Figure 4, top panel). The appearance of such a strong anisotropy in  $\text{Sr}_2\text{RuO}_4$  was not obvious *a priori*, as the third FS, arising from the  $\gamma$  band, is fairly isotropic.

*Conclusion*— We have presented a framework to construct the full Boltzmann collision operator for metals based on combining numerical calculations with transport and acoustic attenuation measurements. We obtain strong quantitative agreement with the measured resistivity and viscosity in  $\text{Sr}_2\text{RuO}_4$ , and provide predictions for the non-local conductivity. In the future, it will be interesting to study how these properties evolve under strain as  $\text{Sr}_2\text{RuO}_4$  crosses a Lifshitz transition, following earlier work [65–74, 104, 105]. More broadly, this framework can be applied to a variety of other materials and to other properties that depend sensitively on the fine features of the collision operator, including thermal [106] and magnetotransport [107].

The work of D.T. and T.S. was supported by the U.S. Department of Energy, Office of Science, Office of Basic Energy Sciences under Award Number DE-SC0025568. B.J.R. and S.G. acknowledge support for building the experiment, collecting and analyzing the data, and writing the manuscript from the Office of Basic Energy Sciences of the United States Department of Energy under award no. DE-SC0020143. We gratefully acknowledge Christian Lupien for providing the resistivity data below 2 K measured in a magnetic field, as well as providing information about their previously-published resistivity and viscosity data. We gratefully acknowledge discussions with Avi Shragai, Aaron Hui, Andrew Mackenzie, Graham Baker, and Veronika Sunko. Simulation codes are available on Github in the form of the package Ludwig.jl

v0.1.0 [108].

\* bradramshaw@cornell.edu

† tscaffid@uci.edu

- [1] L. D. Landau and E. M. Lifshitz, *Fluid Mechanics, Second Edition: Volume 6 (Course of Theoretical Physics)* (Butterworth-Heinemann, 1987).
- [2] R. N. Gurzhi, *Soviet Physics Uspekhi* **11**, 255 (1968).
- [3] A. Tomadin, G. Vignale, and M. Polini, *Physical Review Letters* **113**, 235901 (2014).
- [4] L. Levitov and G. Falkovich, *Nature Physics* **12**, 672 (2016/07/01, 2016).
- [5] J. Zaanen, *Science* **351**, 1026 (2016).
- [6] A. Lucas and S. A. Hartnoll, *Physical Review B* **97**, 045105 (2018).
- [7] A. Lucas and K. C. Fong, *Journal of Physics: Condensed Matter* **30**, 053001 (2018).
- [8] D. Svintsov, *Physical Review B* **97**, 121405 (2018).
- [9] A. Shytov, J. F. Kong, G. Falkovich, and L. Levitov, *Physical Review Letters* **121**, 176805 (2018).
- [10] X. Huang and A. Lucas, *Physical Review B* **103**, 155128 (2021).
- [11] B. N. Narozhny, I. V. Gornyi, A. D. Mirlin, and J. Schmalian, *Annalen der Physik* **529**, 1700043 (2017).
- [12] B. N. Narozhny, *Annals of Physics* **411**, 167979 (2019).
- [13] A. Levchenko and J. Schmalian, *Annals of Physics* **419**, 168218 (2020).
- [14] L. Fritz and T. Scaffidi, *Annual Review of Condensed Matter Physics* **15**, 17 (2024).
- [15] Z. Z. Yu, M. Haerle, J. W. Zwart, J. Bass, W. P. Pratt, and P. A. Schroeder, *Physical Review Letters* **52**, 368 (1984).
- [16] J. E. Black, *Physical Review B* **21**, 3279 (1980).
- [17] L. W. Molenkamp and M. J. M. de Jong, *Physical Review B* **49**, 5038 (1994).
- [18] D. A. Bandurin, I. Torre, R. K. Kumar, M. Ben Shalom, A. Tomadin, A. Principi, G. H. Auton, E. Khestanova, K. S. Novoselov, I. V. Grigorieva, L. A. Ponomarenko, A. K. Geim, and M. Polini, *Science* **351**, 1055 (2016).
- [19] P. J. W. Moll, P. Kushwaha, N. Nandi, B. Schmidt, and A. P. Mackenzie, *Science* **351**, 1061 (2016).
- [20] P. S. Alekseev, *Physical Review Letters* **117**, 166601 (2016).
- [21] R. Krishna Kumar, D. A. Bandurin, F. M. D. Pellegrino, Y. Cao, A. Principi, H. Guo, G. H. Auton, M. Ben Shalom, L. A. Ponomarenko, G. Falkovich, K. Watanabe, T. Taniguchi, I. V. Grigorieva, L. S. Levitov, M. Polini, and A. K. Geim, *Nature Physics* **13**, 1182 (2017).
- [22] T. Scaffidi, N. Nandi, B. Schmidt, A. P. Mackenzie, and J. E. Moore, *Physical Review Letters* **118**, 226601 (2017).
- [23] T. Holder, R. Queiroz, T. Scaffidi, N. Silberstein, A. Rozen, J. A. Sulpizio, L. Ella, S. Ilani, and A. Stern, *Physical Review B* **100**, 245305 (2019).
- [24] M. Shavit, A. Shytov, and G. Falkovich, *Physical Review Letters* **123**, 026801 (2019).
- [25] J. A. Sulpizio, L. Ella, A. Rozen, J. Birkbeck, D. J. Perello, D. Dutta, M. Ben-Shalom, T. Taniguchi, K. Watanabe, T. Holder, R. Queiroz, A. Principi, A. Stern, T. Scaffidi, A. K. Geim, and S. Ilani, *Nature* **576**, 75 (2019/12/01, 2019).
- [26] A. I. Berdyugin, S. G. Xu, F. M. D. Pellegrino, R. Krishna Kumar, A. Principi, I. Torre, M. Ben Shalom, T. Taniguchi, K. Watanabe, I. V. Grigorieva, M. Polini, A. K. Geim, and D. A. Bandurin, *Science* **364**, 162 (2019).
- [27] A. Stern, T. Scaffidi, O. Reuven, C. Kumar, J. Birkbeck, and S. Ilani, *Physical Review Letters* **129**, 157701 (2022).
- [28] A. Aharon-Steinberg, T. Völkl, A. Kaplan, A. K. Pariari, I. Roy, T. Holder, Y. Wolf, A. Y. Meltzer, Y. Myasoedov, M. E. Huber, B. Yan, G. Falkovich, L. S. Levitov, M. Hücker, and E. Zeldov, *Nature* **607**, 74 (2022/07/01, 2022).
- [29] C. Kumar, J. Birkbeck, J. A. Sulpizio, D. Perello, T. Taniguchi, K. Watanabe, O. Reuven, T. Scaffidi, A. Stern, A. K. Geim, and S. Ilani, *Nature* **609**, 276 (2022).
- [30] E. I. Kiselev and J. Schmalian, *Physical Review B* **99**, 035430 (2019).
- [31] A. Lucas, *Physical Review B* **95**, 115425 (2017).
- [32] R. Moessner, N. Morales-Durán, P. Surówka, and P. Witkowski, *Physical Review B* **100**, 155115 (2019).
- [33] K. G. Nazaryan and L. Levitov, *Physical Review B* **110**, 045147 (2024).
- [34] P. S. Alekseev and M. A. Semina, *Physical Review B* **98**, 165412 (2018).
- [35] C. Lupien, *Ultrasound Attenuation in the Unconventional Superconductor Sr<sub>2</sub>RuO<sub>4</sub>*, Ph.D. thesis, University of Toronto (2002).
- [36] C. Lupien, W. A. MacFarlane, C. Proust, L. Taillefer, Z. Q. Mao, and Y. Maeno, *Physical Review Letters* **86**, 5986 (2001).
- [37] T. Holstein, *Physical Review* **113**, 479 (1959).
- [38] F. S. Khan and P. B. Allen, *Physical Review B* **35**, 1002 (1987).
- [39] R. S. Sorbello, *physica status solidi (b)* **77**, 141 (1976).
- [40] M. S. Steinberg, *Phys. Rev.* **109**, 1486 (1958).
- [41] A. B. Bhatia and R. A. Moore, *Phys. Rev.* **121**, 1075 (1961).
- [42] T. M. Rice and L. J. Sham, *Physical Review B* **1**, 4546 (1970).
- [43] S. Sathish, S. Chatterjee, O. N. Awasthi, and E. S. R. Gopal, *Journal of Low Temperature Physics* **63**, 423 (1986).
- [44] R. J. Kolouch and K. A. McCarthy, *Physical Review* **139**, A700 (1965).
- [45] D. H. Filson, *Physical Review* **115**, 1516 (1959).
- [46] M. Kaveh and N. Wiser, *Advances in Physics* **33**, 257 (1984), <https://doi.org/10.1080/00018738400101671>.
- [47] J. Ziman, *Electrons and Phonons: The Theory of Transport Phenomena in Solids*, International Series of Monographs on Physics (OUP Oxford, 2001).
- [48] J. Callaway, *Physical Review* **113**, 1046 (1959).
- [49] P. Ledwith, H. Guo, A. Shytov, and L. Levitov, *Physical Review Letters* **123**, 116601 (2019).
- [50] P. J. Ledwith, H. Guo, and L. Levitov, *Annals of Physics* **411**, 167913 (2019).
- [51] G. Baker, M. Moravec, and A. P. Mackenzie, *Annalen der Physik* **536**, 2400087 (2024).
- [52] J. Hofmann and S. Das Sarma, *Physical Review B* **106**, 205412 (2022).
- [53] Q. Hong, M. Davydova, P. J. Ledwith, and

- L. Levitov, arXiv e-prints , arXiv:2012.03840 (2020), [arXiv:2012.03840](https://arxiv.org/abs/2012.03840) [cond-mat.mes-hall].
- [54] J. Hofmann and U. Gran, arXiv e-prints , arXiv:2210.16300 (2022), [arXiv:2210.16300](https://arxiv.org/abs/2210.16300) [cond-mat.mes-hall].
- [55] A. A. Abrikosov and I. M. Khalatnikov, Reports on Progress in Physics **22**, 329 (1959).
- [56] J. Sykes and G. Brooker, *Annals of Physics* **56**, 1 (1970).
- [57] S. Ahn and S. Das Sarma, *Physical Review B* **106**, L081303 (2022).
- [58] A. Gupta, J. J. Heremans, G. Kataria, M. Chandra, S. Fallahi, G. C. Gardner, and M. J. Manfra, *Physical Review Letters* **126**, 076803 (2021).
- [59] S. A. Hartnoll and A. P. Mackenzie, *Reviews of Modern Physics* **94**, 041002 (2022).
- [60] X. Lin, B. Fauqué, and K. Behnia, *Science* **349**, 945 (2015), <https://www.science.org/doi/pdf/10.1126/science.aaa8655>.
- [61] F. Sun, S. Mishra, U. Stockert, R. Daou, N. Kikugawa, R. S. Perry, E. Hassinger, S. A. Hartnoll, A. P. Mackenzie, and V. Sunko, *Proceedings of the National Academy of Sciences* **121**, e2318159121 (2024), <https://www.pnas.org/doi/pdf/10.1073/pnas.2318159121>.
- [62] A. P. Mackenzie and Y. Maeno, *Rev. Mod. Phys.* **75**, 657 (2003).
- [63] A. P. Mackenzie, T. Scaffidi, C. W. Hicks, and Y. Maeno, *npj Quantum Materials* **2**, 1 (2017).
- [64] C. Bergemann, A. P. Mackenzie, S. R. Julian, D. Forsythe, and E. Ohmichi, *Advances in Physics* **52**, 639 (2003).
- [65] F. Herman, J. Buhmann, M. H. Fischer, and M. Sigrist, *Physical Review B* **99**, 184107 (2019).
- [66] C. W. Hicks, D. O. Brodsky, E. A. Yelland, A. S. Gibbs, J. A. N. Bruin, M. E. Barber, S. D. Edkins, K. Nishimura, S. Yonezawa, Y. Maeno, and A. P. Mackenzie, *Science* **344**, 283 (2014).
- [67] A. Steppke, L. Zhao, M. E. Barber, T. Scaffidi, F. Jerzembeck, H. Rosner, A. S. Gibbs, Y. Maeno, S. H. Simon, A. P. Mackenzie, and C. W. Hicks, *Science* **355**, eaaf9398 (2017), <https://www.science.org/doi/pdf/10.1126/science.aaf9398>.
- [68] M. E. Barber, A. S. Gibbs, Y. Maeno, A. P. Mackenzie, and C. W. Hicks, *Phys. Rev. Lett.* **120**, 076602 (2018).
- [69] M. E. Barber, F. Lechermann, S. V. Streltsov, S. L. Skornyakov, S. Ghosh, B. J. Ramshaw, N. Kikugawa, D. A. Sokolov, A. P. Mackenzie, C. W. Hicks, and I. I. Mazin, *Physical Review B* **100**, 245139 (2019).
- [70] V. Sunko, E. Abarca Morales, I. Marković, M. E. Barber, D. Milosavljević, F. Mazzola, D. A. Sokolov, N. Kikugawa, C. Cacho, P. Dudin, H. Rosner, C. W. Hicks, P. D. C. King, and A. P. Mackenzie, *npj Quantum Materials* **4**, 46 (2019).
- [71] Y.-S. Li, M. Garst, J. Schmalian, S. Ghosh, N. Kikugawa, D. A. Sokolov, C. W. Hicks, F. Jerzembeck, M. S. Ikeda, Z. Hu, B. J. Ramshaw, A. W. Rost, M. Nicklas, and A. P. Mackenzie, *Nature* **607**, 276 (2022).
- [72] A. Chronister, M. Zingl, A. Pustogow, Y. Luo, D. A. Sokolov, F. Jerzembeck, N. Kikugawa, C. W. Hicks, J. Mravlje, E. D. Bauer, J. D. Thompson, A. P. Mackenzie, A. Georges, and S. E. Brown, *npj Quantum Materials* **7**, 113 (2022).
- [73] H. M. L. Noad, K. Ishida, Y.-S. Li, E. Gati, V. Stangier, N. Kikugawa, D. A. Sokolov, M. Nicklas, B. Kim, I. I. Mazin, M. Garst, J. Schmalian, A. P. Mackenzie, and C. W. Hicks, *Science* **382**, 447 (2023).
- [74] P.-Y. Yang, H. M. L. Noad, M. E. Barber, N. Kikugawa, D. A. Sokolov, A. P. Mackenzie, and C. W. Hicks, *Phys. Rev. Lett.* **131**, 036301 (2023).
- [75] Above 12 K, phonon-phonon and phonon-dislocation scattering contribute significantly to the acoustic attenuation.
- [76] Note earlier work on Sr<sub>2</sub>RuO<sub>4</sub> focused on transport at higher temperatures within Dynamical Mean Field Theory [109, 110].
- [77] S. Ghosh, A. Shekhter, F. Jerzembeck, N. Kikugawa, D. A. Sokolov, M. Brando, A. P. Mackenzie, C. W. Hicks, and B. J. Ramshaw, *Nature Physics* **17**, 199 (2021).
- [78] S. Ghosh, T. G. Kiely, A. Shekhter, F. Jerzembeck, N. Kikugawa, D. A. Sokolov, A. P. Mackenzie, and B. J. Ramshaw, *Physical Review B* **106**, 024520 (2022).
- [79] M. B. Walker, M. F. Smith, and K. V. Samokhin, *Physical Review B* **65**, 014517 (2001).
- [80] Note that the magnitude of the viscosity reported in Lupien *et al.* [36] is small by a factor of two—this was corrected in Lupien [35] (from Christian Lupien, private communication).
- [81] See supplemental material [url] for additional details on high and low frequency limits for ultrasound spectroscopy, the quasiparticle scattering rate, the discretization scheme for computing the collision operator, the impurity scattering model, the tight-binding model used, and the deformation potentials, which includes refs. [82, 83].
- [82] F. S. Khan, A. Auerbach, and P. B. Allen, *Solid State Communications* **54**, 135 (1985).
- [83] B. Burganov, C. Adamo, A. Mulder, M. Uchida, P. D. C. King, J. W. Harter, D. E. Shai, A. S. Gibbs, A. P. Mackenzie, R. Uecker, M. Bruetzam, M. R. Beasley, C. J. Fennie, D. G. Schlom, and K. M. Shen, *Physical Review Letters* **116**, 197003 (2016).
- [84] J. M. Buhmann, *Unconventional Transport Properties of Correlated Two-Dimensional Fermi Liquids*, *Doctoral Thesis*, ETH Zurich (2013).
- [85] In which case,  $\langle \mathbf{k}_1 | V_{\text{imp}} | \mathbf{k}_2 \rangle$  is the  $T_{\mathbf{k}_1, \mathbf{k}_2}$  matrix, strictly speaking [111].
- [86] M. Suzuki, M. A. Tanatar, N. Kikugawa, Z. Q. Mao, Y. Maeno, and T. Ishiguro, *Physical Review Letters* **88**, 227004 (2002).
- [87] N. Kikugawa, A. P. Mackenzie, and Y. Maeno, Effects of In-Plane Impurity Substitution in Sr<sub>2</sub>RuO<sub>4</sub> (2002), [arXiv:cond-mat/0210190](https://arxiv.org/abs/cond-mat/0210190).
- [88] I. R. Lapidus, *American Journal of Physics* **50**, 45 (1982), [https://pubs.aip.org/aapt/ajp/article-pdf/50/1/45/11591236/45\\_1\\_online.pdf](https://pubs.aip.org/aapt/ajp/article-pdf/50/1/45/11591236/45_1_online.pdf).
- [89] V. Sunko, P. H. McGuinness, C. S. Chang, E. Zhakina, S. Khim, C. E. Dreyer, M. Konczykowski, H. Borrmann, P. J. W. Moll, M. König, D. A. Muller, and A. P. Mackenzie, *Physical Review X* **10**, 021018 (2020).
- [90] The deformation potentials are calculated based on the strain dependence as inferred from uniaxial strain experiments [69, 73] (see SM for more details).
- [91] This is contrast to Ref. [65] which only included the  $\gamma$  band.
- [92] G. Baker, D. Valentinis, and A. P. Mackenzie, *Low Temperature Physics* **49**, 1338 (2023).
- [93] K. Agarwal, R. Schmidt, B. Halperin, V. Oganesyan, G. Zaránd, M. D. Lukin, and E. Demler, *Physical Re-*

- view B **95**, 155107 (2017).
- [94] S. Kolkowitz, A. Safira, A. A. High, R. C. Devlin, S. Choi, Q. P. Unterreithmeier, D. Patterson, A. S. Zibrov, V. E. Manucharyan, H. Park, and M. D. Lukin, *Science* **347**, 1129 (2015).
- [95] G. E. H. Reuter, E. H. Sondheimer, and A. H. Wilson, *Proceedings of the Royal Society of London. Series A. Mathematical and Physical Sciences* **195**, 336 (1948).
- [96] D. Forcella, J. Zaanen, D. Valentinis, and D. van der Marel, *Physical Review B* **90**, 035143 (2014).
- [97] P. Matus, R. M. A. Dantas, R. Moessner, and P. Surówka, *Proceedings of the National Academy of Sciences* **119**, e2200367119 (2022).
- [98] D. Valentinis, G. Baker, D. A. Bonn, and J. Schmalian, *Physical Review Research* **5**, 013212 (2023).
- [99] A. P. Mackenzie, *Reports on Progress in Physics* **80**, 032501 (2017).
- [100] N. Nandi, T. Scaffidi, P. Kushwaha, S. Khim, M. E. Barber, V. Sunko, F. Mazzola, P. D. C. King, H. Rosner, P. J. W. Moll, M. König, J. E. Moore, S. Hartnoll, and A. P. Mackenzie, *npj Quantum Materials* **3**, 1 (2018), publisher: Nature Publishing Group.
- [101] C. Q. Cook and A. Lucas, *Phys. Rev. B* **99**, 235148 (2019).
- [102] M. D. Bachmann, A. L. Sharpe, G. Baker, A. W. Barnard, C. Putzke, T. Scaffidi, N. Nandi, P. H. McGuinness, E. Zhakina, M. Moravec, S. Khim, M. König, D. Goldhaber-Gordon, D. A. Bonn, A. P. Mackenzie, and P. J. W. Moll, *Nature Physics* **18**, 819 (2022).
- [103] G. Baker, T. W. Branch, J. S. Bobowski, J. Day, D. Valentinis, M. Oudah, P. McGuinness, S. Khim, P. Surówka, Y. Maeno, T. Scaffidi, R. Moessner, J. Schmalian, A. P. Mackenzie, and D. A. Bonn, *Physical Review X* **14**, 011018 (2024).
- [104] C. H. Mousatov, E. Berg, and S. A. Hartnoll, *Proceedings of the National Academy of Sciences* **117**, 2852 (2020), <https://www.pnas.org/doi/pdf/10.1073/pnas.1915224117>.
- [105] V. C. Stangier, E. Berg, and J. Schmalian, *Phys. Rev. B* **105**, 115113 (2022).
- [106] S. Jiang, B. Fauqué, and K. Behnia, *Phys. Rev. Lett.* **131**, 016301 (2023).
- [107] G. Grissonnanche, Y. Fang, A. Legros, S. Verret, F. Laliberté, C. Collignon, J. Zhou, D. Graf, P. A. Goddard, L. Taillefer, and B. J. Ramshaw, *Nature* **595**, 667 (2021).
- [108] Davis Thuillier, *Ludwig.jl* (2024).
- [109] X. Deng, K. Haule, and G. Kotliar, *Physical Review Letters* **116**, 256401 (2016).
- [110] D. J. Abramovitch, J.-J. Zhou, J. Mravlje, A. Georges, and M. Bernardi, *Physical Review Materials* **7**, 093801 (2023).
- [111] A. C. Hewson, *The Kondo Problem to Heavy Fermions*, Cambridge Studies in Magnetism (Cambridge University Press, 1993).

## End Matter

*Experimental Methods*— To access the long-wavelength limit of sound attenuation in  $\text{Sr}_2\text{RuO}_4$ , we used resonant ultrasound spectroscopy (RUS). We measured all six elastic moduli and their respective attenuation coefficients, from 1.2 K to 12 K, of a single-crystal  $\text{Sr}_2\text{RuO}_4$  sample with a  $T_c$  of 1.43 K. The measurement frequency is approximately 2 MHz. The details of the experimental procedure, including sample characterization, are given in Ghosh *et al.* [77]. The details of extracting the sound attenuation and viscosity from the resonance linewidths are given in Ghosh *et al.* [78].

*Difference between acoustic and transport viscosity*— In this appendix, we highlight how two different definitions of viscosities appear in the context of acoustic attenuation and non-local transport. Although they both ultimately are written in terms of the collision operator and involve calculating expectation values with distribution functions in the same symmetry sector, the distributions involved are different in the two cases, leading in general to a parametric difference between them. Schematically, we will show that the acoustic viscosity is given by

$$\eta_{\alpha\beta\gamma\delta}^{\text{ac}} \sim \langle D_{\alpha\beta} | L^{-1} | D_{\gamma\delta} \rangle \quad (\text{A1})$$

with  $D$  the deformation potential, whereas the transport viscosity reads

$$\eta_{\alpha\beta\gamma\delta}^{\text{tr}} \sim \langle mv_{\alpha}v_{\beta} | L^{-1} | mv_{\gamma}v_{\delta} \rangle \quad (\text{A2})$$

with  $m$  an average effective mass defined below. The acoustic and transport viscosities are thus related to expectation values of the collision operator for states given by  $|D_{\alpha\beta}\rangle$  and  $|mv_{\alpha}v_{\beta}\rangle$  respectively, which have the same units and the same symmetry, but can in general be parametrically different since  $D$  is given by the derivative of the energy with strain, whereas  $v$  is related to the derivative of the energy with  $\mathbf{k}$ .

A simple illustrative example is to consider a nearest-neighbor 1D hopping model for which the hopping amplitude depends on the strain  $\epsilon$  as  $t(\epsilon) = t(1 - \alpha\epsilon)$ , with  $\alpha$  a dimensionless number. In this case, one finds  $D \propto t\alpha \cos(k_F)$  but  $mv^2 \propto tk_F |\sin(k_F)|$ . Clearly these two distributions have a different parametric dependence on the model parameters: e.g. when  $k_F \simeq \pi/2$ ,  $D$  is parametrically small whereas  $mv^2$  is not. Further, the deformation potentials depend on the strength of the electron-phonon coupling, which shows up in a tight-binding model as dimensionless numbers giving the hopping dependence on strain, e.g.  $\alpha$  in the example above. By contrast,  $|mv_{\alpha}v_{\beta}\rangle$  is impervious to the electron-phonon coupling. For the simple example above, this means  $\eta^{\text{ac}} \propto \alpha^2$ , whereas  $\eta^{\text{tr}}$  is independent of  $\alpha$ . Since  $\alpha$  can in general be large (we used  $\alpha \simeq 7$  in our  $\text{Sr}_2\text{RuO}_4$  model for nearest-neighbor hopping), this can lead to orders of magnitude difference between the two viscosities.

Let us now derive the formulas above for the two vis-

cosities. First, in the main text we have given the following formula for the acoustic viscosity [38]:

$$\eta^{\text{ac}} = \langle D|L^{-1}|D \rangle \quad (\text{A3})$$

with  $D_{\alpha\beta} = \partial E/\partial S_{\alpha\beta}$  the deformation potentials. (We drop factors of 2 for spin in this End Matter.)

As explained in the main text, a ‘‘transport viscosity’’ appears in non-local electric transport, through the small- $q$  decay of  $\sigma(q)$ :

$$\nu^{\text{tr}} = \frac{1}{\tau_\sigma} q_0^{-2} \equiv \frac{1}{\tau_\sigma} \frac{1}{\sigma(0)} \left| \frac{\partial \sigma(q)}{\partial q^2} \right|_{q=0} \quad (\text{A4})$$

where  $q_0$  is the inverse Gurzhi length and  $\tau_\sigma$  is the effective mean free time giving the bulk conductivity. This viscosity naturally appears as a kinematic viscosity in units of meters squared per second. By expanding

$$\sigma_{\alpha\beta}(\mathbf{q}) = e^2 \langle v_\alpha | (L + i\mathbf{q} \cdot \mathbf{v})^{-1} | v_\beta \rangle \quad (\text{A5})$$

in powers of  $i\mathbf{q} \cdot \mathbf{v}$ , one finds

$$\nu^{\text{tr}} = \frac{\langle v_\perp | L^{-1} v_\parallel L^{-1} v_\parallel L^{-1} | v_\perp \rangle}{\langle v_\perp | L^{-1} | v_\perp \rangle^2 \langle v_\perp | v_\perp \rangle^{-1}} \quad (\text{A6})$$

where  $v_\perp$  and  $v_\parallel$  are respectively perpendicular and parallel to  $\mathbf{q}$ . The numerator involves three factors of  $L^{-1}$  and thus in general cannot be expressed in terms of an expectation value of a single factor of  $L^{-1}$  as  $\eta^{\text{ac}}$  could.

It is however instructive to consider the case when  $|v_\perp\rangle$  is close to an eigenvector of  $L$  (which is exactly true for a circular FS), i.e.  $L^{-1}|v_\perp\rangle \simeq \tau_\sigma|v_\perp\rangle$ , in which case

$$\nu^{\text{tr}} \simeq \frac{\langle v_\perp v_\parallel | L^{-1} | v_\perp v_\parallel \rangle}{\langle v_\perp | v_\perp \rangle} \quad (\text{A7})$$

Now, to obtain a dynamic viscosity, we add a factor of mass density  $nm$  with  $n$  the carrier density and  $m \equiv n\langle v_\perp | v_\perp \rangle^{-1}$  the average effective mass, leading to

$$\eta^{\text{tr}} \simeq \langle m v_\perp v_\parallel | L^{-1} | m v_\perp v_\parallel \rangle \quad (\text{A8})$$

which takes the form given in (A2). (One can check that the definition for the mass above gives  $m = k_F/v_F$  for a circular Fermi surface).

Finally, we give for completeness the formulas for  $\mathbf{q}$  along (100), which corresponds to  $B_{2g}$ :

$$\eta_{100}^{\text{tr}} \simeq \langle m v_x v_y | L^{-1} | m v_x v_y \rangle \quad (\text{A9})$$

and for  $\mathbf{q}$  along 110, which corresponds to  $B_{1g}$ :

$$\eta_{110}^{\text{tr}} \simeq \langle m \frac{1}{2}(v_x^2 - v_y^2) | L^{-1} | m \frac{1}{2}(v_x^2 - v_y^2) \rangle \quad (\text{A10})$$

**Supplemental material to “Multipolar Fermi Surface Deformations in  $Sr_2RuO_4$  Probed by Resistivity and Sound Attenuation: A Window into Electron Viscosity and the Collision Operator”**

**Appendix A: Definition of the high and low-frequency limits of sound attenuation**

Sound attenuation in the short-wavelength (“quantum”) limit is dominated by the direct production of particle-hole pairs by ultrasonic phonons [38]. This limit is reached when the product of the sound wavevector  $q$  and electron mean free path  $l$  is of order 1. In  $Sr_2RuO_4$ , which has an electron mean free path of order  $1 \mu\text{m}$  and a  $B_{1g}$  shear sound velocity of  $3 \text{ km/s}$ , this crossover occurs at around  $500 \text{ MHz}$ . The resonant ultrasound data used in this manuscript were taken at  $\approx 2 \text{ MHz}$  are therefore well below this limit and in the “hydrodynamic” regime of sound attenuation [38].

Previous measurements of the  $B_{1g}$  sound attenuation in  $Sr_2RuO_4$ , such as Lupien *et al.* [36], were performed at higher frequencies using the pulse echo ultrasound technique. Therefore, they may contain sizable contributions from particle-hole pair production. We find, however, that at least for the  $B_{1g}$  viscosity, our resonant ultrasound measurements performed at  $\approx 2 \text{ MHz}$  are in good quantitative agreement with those of Lupien *et al.* [36] measured by pulse-echo ultrasound at  $\approx 40 \text{ MHz}$ .

**Appendix B: Scattering Rate**

Our calculation of the collision operator is a generalization of the method employed in [84] to a material with multiple bands. The electron-electron collision operator has been calculated previously for the  $\gamma$  band of  $Sr_2RuO_4$  in Herman *et al.* [65] using this approach in order to consider how transport coefficients deviate from expected Fermi liquid behavior when a band undergoes a Lifshitz transition. However, for comparing the conductivity and the viscosity, it is necessary to capture how the  $\alpha$  and  $\beta$  contribute with a greater weight to the conductivity than the viscosity due to  $D_{B_{1g}}$  being smaller on these bands compared to the  $\gamma$  band.

The low-energy physics of electrons in the  $d$ -orbitals of the ruthenium atoms in  $Sr_2RuO_4$  is modeled by the following Hamiltonian,

$$H = H_0 + H_{\text{int}} \quad (\text{A1})$$

$$H_0 = - \sum_{ij\sigma} \sum_{ab} t_{ij}^{ab} c_{ia\sigma}^\dagger c_{jb\sigma} - \mu \sum_{ia\sigma} n_{ia\sigma} \quad (\text{A2})$$

$$H_{\text{int}} = \frac{U_{\text{ee}}}{2} \sum_{i\sigma} \sum_{ab} n_{ia\sigma} n_{ib-\sigma} + \frac{U_{\text{ee}}}{2} \sum_{i\sigma} \sum'_{ab} n_{ia\sigma} n_{ib\sigma} \quad (\text{A3})$$

where  $t_{ij}^{ab}$  is effective hopping between site  $j$  in orbital  $b$  and site  $i$  in orbital  $a$ ,  $U_{\text{ee}}$  characterizes the strength of onsite Coulomb repulsion, and the prime in the summation of the latter term of  $H_{\text{int}}$  indicates that the term  $a = b$  is excluded. The kinetic Hamiltonian can be diagonalized at each point in  $k$ -space as

$$H_0 = \sum_{k\mu\sigma} \varepsilon_{k\mu} c_{k\mu\sigma}^\dagger c_{k\mu\sigma} \quad (\text{A4})$$

where  $\mu$  denotes a *band index*. For each  $\mathbf{k}$ , there exists  $U_{\mathbf{k}}^{a\mu}$  such that  $c_{\mathbf{k}a} = U_{\mathbf{k}}^{a\mu} c_{\mathbf{k}\mu}$ . Expressing the interaction term in this basis, we obtain

$$H_{\text{int}} = \frac{U_{\text{ee}}}{N} \sum_{\mathbf{k}_1, \mathbf{k}_2, \mathbf{q}} \sum_{\sigma_1, \sigma_2} \sum_{\mu\nu\eta\tau} c_{\mathbf{k}_1 - \mathbf{q}\eta\sigma_1}^\dagger F_{\mathbf{k}_1 - \mathbf{q}, \mathbf{k}_1}^{\eta\mu} c_{\mathbf{k}_1\mu\sigma_1} c_{\mathbf{k}_2 + \mathbf{q}\tau\sigma_2}^\dagger F_{\mathbf{k}_2 + \mathbf{q}, \mathbf{k}_2}^{\tau\nu} c_{\mathbf{k}_2\nu\sigma_2} \quad (\text{A5})$$

where  $F_{\mathbf{k}_1, \mathbf{k}_2}^{\mu\nu} \equiv \left( U_{\mathbf{k}_1}^\dagger U_{\mathbf{k}_2} \right)^{\mu\nu}$ .

Since the interaction does not change spin, we can define the spinless quasiparticle interaction vertex as

$$W_{\mu_1, \mu_2, \mu_3, \mu_4}(\mathbf{k}_1, \mathbf{k}_2, \mathbf{k}_3, \mathbf{k}_4) = \langle \mathbf{k}_1, \mu_1, \mathbf{k}_2, \mu_2 | \hat{W} | \mathbf{k}_3, \mu_3, \mathbf{k}_4, \mu_4 \rangle \quad (\text{A6})$$

$$= U_{\text{ee}} F_{\mathbf{k}_3, \mathbf{k}_1}^{\mu_3\mu_1} F_{\mathbf{k}_4, \mathbf{k}_2}^{\mu_4\mu_2}. \quad (\text{A7})$$

As in [84], the scattering rates are taken to be given by Fermi's golden rule with an antisymmetrized scattering vertex to account for the anticommutativity of fermions as

$$\Gamma_{\mu_1\mu_2\mu_3\mu_4}^{\sigma_1\sigma_2\sigma_3\sigma_4}(\mathbf{k}_1, \mu_1, \mathbf{k}_2, \mu_2, \mathbf{k}_3, \mu_3, \mathbf{k}_4, \mu_4) = \frac{2\pi}{\hbar} \delta(\varepsilon_{\mu_1}(\mathbf{k}_1) + \varepsilon_{\mu_2}(\mathbf{k}_2) - \varepsilon_{\mu_3}(\mathbf{k}_3) - \varepsilon_{\mu_4}(\mathbf{k}_4)) (2\pi)^2 \delta(\mathbf{k}_1 + \mathbf{k}_2 - \mathbf{k}_3 - \mathbf{k}_4) \\ \times \frac{1}{2} \left| W_{\mu_1, \mu_2, \mu_3, \mu_4}^{\sigma_1, \sigma_2, \sigma_3, \sigma_4}(\mathbf{k}_1, \mathbf{k}_2, \mathbf{k}_3, \mathbf{k}_4) - W_{\mu_1, \mu_2, \mu_4, \mu_3}^{\sigma_1, \sigma_2, \sigma_4, \sigma_3}(\mathbf{k}_1, \mathbf{k}_2, \mathbf{k}_4, \mathbf{k}_3) \right|^2. \quad (\text{A8})$$

Summing over spin polarizations and band indices, we can obtain an effective scattering rate

$$\Gamma^{\text{eff}}(\mathbf{k}_1, \mathbf{k}_2, \mathbf{k}_3, \mathbf{k}_4) = \sum_{\mu_1\mu_2\mu_3\mu_4} \left( \Gamma_{\mu_1\mu_2\mu_3\mu_4}^{\sigma\sigma\sigma\sigma}(\mathbf{k}_1, \mathbf{k}_2, \mathbf{k}_3, \mathbf{k}_4) + 2\Gamma_{\mu_1\mu_2\mu_3\mu_4}^{\sigma-\sigma-\sigma\sigma}(\mathbf{k}_1, \mathbf{k}_2, \mathbf{k}_3, \mathbf{k}_4) \right) \quad (\text{A9})$$

which accords with an effective vertex

$$W_{\text{eff}}^2(\mathbf{k}_1, \mu_1, \mathbf{k}_2, \mu_2, \mathbf{k}_3, \mu_3, \mathbf{k}_4, \mu_4) = U_{\text{ee}}^2 \left( |F_{\mathbf{k}_3, \mathbf{k}_1}^{\mu_3, \mu_1} F_{\mathbf{k}_4, \mathbf{k}_2}^{\mu_4, \mu_2} - F_{\mathbf{k}_4, \mathbf{k}_1}^{\mu_4, \mu_1} F_{\mathbf{k}_3, \mathbf{k}_2}^{\mu_3, \mu_2}|^2 + 2|F_{\mathbf{k}_4, \mathbf{k}_1}^{\mu_4, \mu_1} F_{\mathbf{k}_3, \mathbf{k}_2}^{\mu_3, \mu_2}|^2 \right) \quad (\text{A10})$$

such that

$$\Gamma^{\text{eff}}(\mathbf{k}_1, \mathbf{k}_2, \mathbf{k}_3, \mathbf{k}_4) = \frac{\pi}{\hbar} (2\pi)^2 \delta(\mathbf{k}_1 + \mathbf{k}_2 - \mathbf{k}_3 - \mathbf{k}_4) \\ \times \sum_{\mu_1\mu_2\mu_3\mu_4} \delta(\varepsilon_{\mu_1}(\mathbf{k}_1) + \varepsilon_{\mu_2}(\mathbf{k}_2) - \varepsilon_{\mu_3}(\mathbf{k}_3) - \varepsilon_{\mu_4}(\mathbf{k}_4)) \\ \times W_{\text{eff}}^2(\mathbf{k}_1, \mu_1, \mathbf{k}_2, \mu_2, \mathbf{k}_3, \mu_3, \mathbf{k}_4, \mu_4). \quad (\text{A11})$$

In practice, our calculations are performed at sufficiently low temperatures such that for each  $\mathbf{k}$  there is a unique band index  $\mu$  such that for all  $\nu \neq \mu$ ,  $f^{(0)}(\varepsilon_\nu(\mathbf{k}))(1 - f^{(0)}(\varepsilon_\nu(\mathbf{k}))) \ll 1$ . Therefore, we will drop the sum over band indices, and the band index used for calculating energies will be implicit in  $\mathbf{k}$ . That is, the problem effectively reduces to the single band case, with the dispersion given as a piecewise function on implicit regions of the first Brillouin zone.

### Appendix C: Discretization of the Collision Operator

Discretizing the Brillouin zone allows us to express the action of the collision integral upon an out-of-equilibrium distribution function as the following matrix equation.

$$L[\chi(\mathbf{k})]_i = \sum_j \mathbf{L}_{ij} \chi_j \\ \mathbf{L}_{ij} = \frac{1}{dV_i} \int_i \frac{d^2\mathbf{k}_i}{(2\pi)^2} \int_j \frac{d^2\mathbf{k}_j}{(2\pi)^2} \mathcal{L}(\mathbf{k}_i, \mathbf{k}_j) \quad (\text{A1})$$

where  $\int_i$  denotes an integral over the momenta contained in patch  $i$  and  $dV_i$  is the area of patch  $i$ . We adopt the discretization scheme of [84] where patches are defined by binning momenta by energy and angle within an annular region of finite width following the Fermi surface of each band (see Figure 1). While Umklapp scattering and impurity scattering relax momentum, particle number and total energy remain conserved quantities for which the corresponding functions  $\chi_j = 1, \varepsilon_j$  are eigenvectors with vanishing eigenvalue. It follows that  $\sum_j \mathbf{L}_{ij} = 0$ , so that in practice only the off-diagonal elements are calculated, and the diagonal elements are obtained from this sum rule.

In terms of the effective scattering rate of Appendix B, the off-diagonal elements are given by

$$\mathbf{L}_{ij} = \frac{1}{dV_i} \frac{\pi/\hbar}{1 - f_i^{(0)}} \frac{1}{(2\pi)^6} \sum_m \left( W_{\text{eff}}^2(\mathbf{k}_i, \mathbf{k}_j, \mathbf{k}_m, \mathbf{k}_i + \mathbf{k}_j - \mathbf{k}_m) f_j^{(0)} (1 - f_m^{(0)}) \mathcal{K}_{ijm} \right. \\ \left. - (W_{\text{eff}}^2(\mathbf{k}_i, \mathbf{k}_m, \mathbf{k}_j, \mathbf{k}_i + \mathbf{k}_m - \mathbf{k}_j) + W_{\text{eff}}^2(\mathbf{k}_i, \mathbf{k}_m, \mathbf{k}_i + \mathbf{k}_m - \mathbf{k}_j, \mathbf{k}_j)) f_m^{(0)} (1 - f_j^{(0)}) \mathcal{K}_{imj} \right) \quad (\text{A2})$$

with

$$\mathcal{K}_{ijm} = \int_i d^2\mathbf{k}_i \int_j d^2\mathbf{k}_j \int_m d^2\mathbf{k}_m (1 - f^{(0)}(\mathbf{k}_i + \mathbf{k}_j - \mathbf{k}_m)) \delta(\varepsilon(\mathbf{k}_i) + \varepsilon(\mathbf{k}_j) - \varepsilon(\mathbf{k}_m) - \varepsilon(\mathbf{k}_i + \mathbf{k}_j - \mathbf{k}_m)) \quad (\text{A3})$$

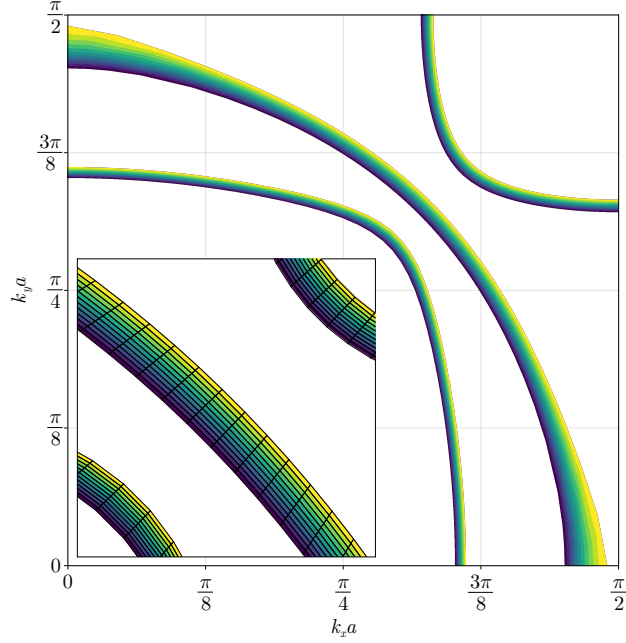


FIG. 1. Fermi surface centered mesh of the first quadrant of the Brillouin zone at 12 K at the sampled resolution. Each annular region has a width of  $12k_B T$ . Inset: Zoom-in on the FSs along 110 to show the mesh.

where all functions outside of patch integrals are approximated as constant within the patch and evaluated at the patch center.

Following [84], we make a coordinate transformation to energy-angle coordinates in each patch and linearize the argument of the delta function with respect to  $\mathbf{k}_i, \mathbf{k}_j, \mathbf{k}_m$ . The integral of (A3) can then be approximated as the volume of intersection of the hyperplane defined by the argument of the delta function with a hypersphere of equal volume to the integration volume, weighted by the value of the integrand on the hyperplane.

The resolution of the mesh is set by three parameters: the width of the annulus, the number  $n_\epsilon$  of energy bins, and the number  $n_\theta$  of angular bins. All simulation data in the main text was generated with an annular width of  $12k_B T$ ,  $n_\epsilon = 11$ , and  $n_\theta = 148$  for each band.

Whereas conservation of particle number is enforced explicitly, the energy eigenvector acquires a small nonzero eigenvalue due to sampling on a finite-width energy window. Figure 2 demonstrates the convergence of the energy eigenvalue compared to those of the longest-lived modes for  $\mathbf{L}_{ee}$ . That the energy eigenvalue decreases while the other eigenvalues increase monotonically with width  $W$  supports that energy will indeed be a zero mode in the limit where the entire Brillouin zone is sampled. For computing the conductivity and viscosity, the corresponding vector has zero overlap with the energy vector, and thus the nonzero energy eigenvalue makes no contribution to either transport coefficient.

#### Appendix D: Electron-impurity scattering

In the unitary limit, for an isotropic 2D band, the matrix element squared for electron-impurity scattering takes the form  $|\langle \mathbf{k}_1 | V_{\text{imp}} | \mathbf{k}_2 \rangle|^2 = 4\hbar^2 v_F^2 / k_F^2$ . We define an analogous Fermi surface-averaged quantity for each band and treat interband scattering by taking the geometric mean of the weights,

$$|\langle \mathbf{k}_1, \mu | V_{\text{imp}} | \mathbf{k}_2, \nu \rangle|^2 = 4 \sqrt{\left( \frac{v_F^2}{k_F^2} \right)_\mu \left( \frac{v_F^2}{k_F^2} \right)_\nu}. \quad (\text{A1})$$

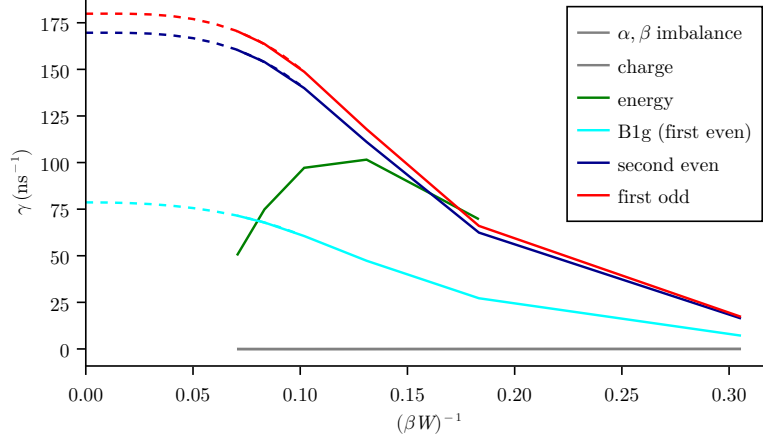


FIG. 2. Convergence of the smallest eigenvalues of the collision operator at  $T = 12$  K with the width  $W$  of the Fermi annulus at constant sampling density in energy of  $T^{-1}$  and  $n_\theta = 148$ . The B1g and “second even” modes are the first two parity-even modes, whereas the “first odd” mode is parity-odd. Dashed lines indicate cubic extrapolation with the convergence criterion  $\lim_{W \rightarrow \infty} d\gamma/d(\beta W)^{-1} = 0$ , which is motivated by the fact, for large enough  $W$ , the entire BZ is sampled and the eigenvalues should thus plateau.

We can also define the average impurity potential

$$|\langle V_{\text{imp}} \rangle|_{\text{av}}^2 = 4 \sqrt[3]{\left(\frac{v_F^2}{k_F^2}\right)_\alpha \left(\frac{v_F^2}{k_F^2}\right)_\beta \left(\frac{v_F^2}{k_F^2}\right)_\gamma} \quad (\text{A2})$$

which serves as a single energy scale for characterizing the impurity strength.

The values of  $v_F, k_F$  for each band from the tight-binding model of [Appendix E](#) are shown in [Table I](#).

Band	$\overline{v_F}$ (m s $^{-1}$ )	$\overline{k_F}$ (nm $^{-1}$ )
$\alpha$	99395	2.97
$\beta$	114577	6.14
$\gamma$	59970	7.39

TABLE I. Fermi-surface-averaged Fermi velocities and Fermi momenta, calculated from the tight-binding model.

### Appendix E: Tight-Binding Model

We use the nearest and next-nearest neighbor tight-binding approximation of the bands presented in [\[83\]](#) where

$$H(\mathbf{k}) = \begin{pmatrix} \epsilon_{xz}(\mathbf{k}) & V(\mathbf{k}) & 0 \\ V(\mathbf{k}) & \epsilon_{yz}(\mathbf{k}) & 0 \\ 0 & 0 & \epsilon_{xy}(\mathbf{k}) \end{pmatrix} \quad (\text{A1})$$

where

$$\begin{aligned} \epsilon_{xy}(\mathbf{k}) &= -\mu_1 - 2t_1 \cos(k_x a) - 2t_1 \cos(k_y a) \\ &\quad - 4t_4 \cos(k_x a) \cos(k_y a) \\ \epsilon_{xz/yz}(\mathbf{k}) &= -\mu_1 - 2t_2 \cos(k_{x/y} a) - 2t_3 \cos(k_{x/y} a) \\ V(\mathbf{k}) &= t_5 \sin(k_x a) \sin(k_y a). \end{aligned} \quad (\text{A2})$$

We take the values found in [\[83\]](#) for  $t_4/t_1, t_3/t_2, t_5/t_2, \mu_1/t_1, \mu_2/t_2$  by fitting to the ARPES Fermi surface, but choose values of  $t_1, t_2^\alpha, t_2^\beta$  which provide best agreement to the cyclotron mass for each band (see [Table II](#)).

$t_1$ (eV)	$t_2^\alpha$ (eV)	$t_2^\beta$ (eV)	$t_4/t_1$	$\mu_1/t$	$t_3/t_2^{\alpha/\beta}$	$t_5/t_2^{\alpha/\beta}$	$\mu_2/t_2^{\alpha/\beta}$
0.0774	0.099	0.128	0.392	1.48	0.08	0.13	1.08

TABLE II. Tight-binding model parameters. Ratios come from [83] with nearest-neighbor hoppings adjusted to provide agreement to the observed cyclotron mass for each band.

### Appendix F: Deformation Potentials

We consider the band deformation potential of [82]

$$D_{\alpha\beta}(\mathbf{k}, \mu) = \left. \frac{\partial \varepsilon((\mathbf{1} - \mathbf{S})\mathbf{k}, \mu)}{\partial S_{\alpha\beta}} \right|_{\mathbf{S}=\mathbf{0}} \quad (\text{A1})$$

where nearest and next-nearest neighbor hopping parameters of the tight-binding model are treated to linear order in strain as

$$\begin{aligned} t_{x/y} &= t_{x/y}^0 (1 - \alpha S_{xx/yy}) \\ t' &= (t')^0 (1 - \alpha' (S_{xx} + S_{yy})/2). \end{aligned} \quad (\text{A2})$$

Here,  $\alpha$  and  $\alpha'$  characterize the rate of deformation. Following [73], we take  $\alpha = \alpha' = 7.604$  which forces the  $\gamma$  band to undergo a Lifshitz transition at a measured longitudinal strain of  $S_{xx} = -0.44\%$  [69].

For sound attenuation in RUS, we are concerned with  $\eta_{\text{B1g}} = \eta_{xxxx} - \eta_{xxyy}$ . Notably,  $\eta_{xxxx} = \eta_{yyyy}$  and  $\eta_{xxyy} = \eta_{yyxx}$  since the linearized collision operator is Hermitian under the inner product defined in the main text, allowing  $\eta_{\text{B1g}}$  to be written in the more symmetric form

$$\begin{aligned} \eta_{\text{B1g}} &= \frac{1}{4} (\eta_{xxxx} - 2\eta_{xxyy} + \eta_{yyyy}) \\ &= \left\langle \frac{D_{xx} - D_{yy}}{2} \middle| L^{-1} \left[ \frac{D_{xx} - D_{yy}}{2} \right] \right\rangle, \end{aligned} \quad (\text{A3})$$

from which we can identify the deformation potential corresponding to B1g strain as

$$D_{\text{B1g}} = \frac{1}{2} (D_{xx} - D_{yy}). \quad (\text{A4})$$